Wall Interference Assessment/Correction for Transonic Airfoil Data

Lawrence L. Green* and Raymond E. Mineck†
NASA Langley Research Center, Hampton, Virginia 23665

Two sets of transonic airfoil data were obtained from the same model tested in both porous, planar-wall and solid, shaped-wall wind tunnels. The published data agree reasonably well with each other but differ significantly from two-dimensional, free-air Navier-Stokes calculations for the same airfoil. An existing computational wall interference assessment/correction (WIAC) procedure was applied to the porous- and shaped-wall data sets. The WIAC corrections generally improve the correlation between the two data sets. Simultaneously, the WIAC corrections also generally improve the correlation between the data and the Navier-Stokes calculations.

Nomenclature

c = model chord
c_d = section drag coefficient
c_n = section normal force coefficient
c_p = pressure coefficient
M = Mach number
Re_c = Reynolds number based on model chord
x = chordwise distance from model leading edge
z = normal direction coordinate
α = angle of attack

Introduction

WIND-TUNNEL test section walls impose artificial constraints on the flow around a model. In the past, analytically derived corrections have been applied to test results to account for these constraints. More recently, computational wall interference assessment/correction techniques, based upon potential flow theory, have been developed to account for these constraints. Alternatively, the artificial constraints can be reduced or possibly eliminated by modifying the flow at the test section boundaries through the use of ventilated- or adaptive-wall test sections. This paper compares the aforementioned techniques for transonic CAST 10-2/DOA 2 airfoil data; this airfoil section was selected because published results[1] indicate that its aerodynamic characteristics are sensitive to small changes in the test conditions.

The model was first tested in the porous-wall National Aeronautical Establishment (NAE) Two-Dimensional High Reynolds Number Facility. The results were corrected for top and bottom wall interference using a classical analytical correction technique. The same model was subsequently tested in the NASA Langley Research Center 0.3-m Transonic Cryogenic Tunnel (TCT) adaptive-wall test section. Both data sets were then corrected with a unified, four-wall, post-test, transonic wall interference assessment/correction (WIAC) technique. Comparisons of the published and WIAC corrected data were made with two-dimensional, free-air Navier-Stokes calculations.

Presented as Paper 90-1406 at the AIAA 16th Aerodynamic Ground Testing Conference, Seattle, WA, June 18-20, 1990; received Nov. 8, 1990; revision received April 5, 1991; accepted for publication April 5, 1991.

*Research Engineer, CAB/FldMD, M/S 128. Senior Member AIAA.
†Research Engineer, TAB/AAD, M/S 361.

Experiments

Description of the Model

The NAE of Canada designed and fabricated a model with a 9-in. (22.86-cm) chord and a CAST 10-2/DOA 2 airfoil section. The airfoil is nominally 12% thick and has a design section normal force coefficient of 0.6 at the design Mach number of 0.765. A sketch of the airfoil section and the upper surface pressure orifice layout are presented in Fig. 1. The orifices were staggered about the model centerline to minimize interference among the neighboring orifices; smaller diameter orifices were used over the forward portion of the model to reduce any orifice size effects where the pressure gradients could be large.

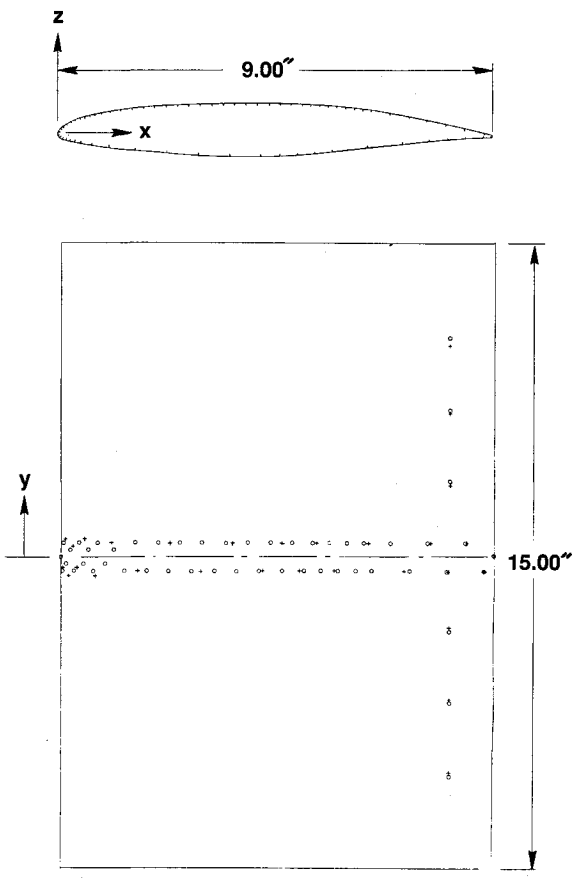

Fig. 1 Sketch of the CAST 10-2/DOA 2 airfoil model and the pressure orifice locations.

Description of the NAE Wind Tunnel

The model was first tested in the NAE Two-Dimensional High Reynolds Number Facility[2,3] to obtain the porous-wall test results[4] reported herein; these data were then corrected[5] for top and bottom wall interference effects, as described in a later section of this paper. A sketch of the NAE Two-Dimensional High Reynolds Number Facility test section is presented in Fig. 2. The test section is 15 in. (38.10 cm) wide and 60 in. (152.40 cm) high with no wall divergence. The sidewalls are solid; the top and bottom walls are porous and covered with a 30 mesh, 40% open screen to reduce the edge-tone noise. The resulting overall porosity of the walls is 8.4%.

The model is mounted on a turntable within an 18-in. (45.72-cm) × 24-in. (60.96-cm) porous panel covered with a woven wire sheet. This porous panel has only a moderate level of suction, intended to control the adverse growth of the boundary layer from the pressure signature imposed on the sidewalls by the model. Normal force coefficients reported herein were deduced from the pressure coefficient measurements, whereas the drag data were computed using the measurements from the total head probe mounted 1.78 chords downstream of the model trailing edge on the test section's centerline.

Description of the NASA Wind Tunnel

The model was subsequently tested in the NASA Langley 0.3-m TCT[6] with the two-dimensional adaptive-wall test section[7] insert. A sketch of the adaptive-wall test section with the plenum sidewall removed is presented in Fig. 3. Although the tunnel includes capability for sidewall boundary-layer control, this capability was not used in the present tests.[8] The test section is 13 in. (33.02 cm) tall × 13 in. (33.02 cm) wide at the entrance. All four walls are solid. The sidewalls are rigid and parallel; the top and bottom walls are flexible and movable with the shape of each wall determined[9] by 21 independent jacks. Pressure orifices are located at each jack position on the centerline of the top and bottom walls. The model is supported between sidewall turntables. Normal force coefficients reported herein were deduced from the pressure coefficient measurements, whereas the drag data were computed using the measurements from the total head probe 1.2 chords behind the model trailing edge on the test section's centerline.

Test Program

Test conditions were selected to emphasize the high subsonic and transonic Mach numbers and the high Reynolds numbers that are possible in the two wind tunnels. The primary goal of these tests was to compare correction techniques for wall interference and not to measure airfoil performance. To eliminate different transition effects between the two data sets, both tests were conducted with transition strips placed on both surfaces of the model. The grit size was determined[10] for a Reynolds number of 10×10^6. Carborundum grit no. 320 with an average grit size of 0.0011 in. (0.03 cm) was used for

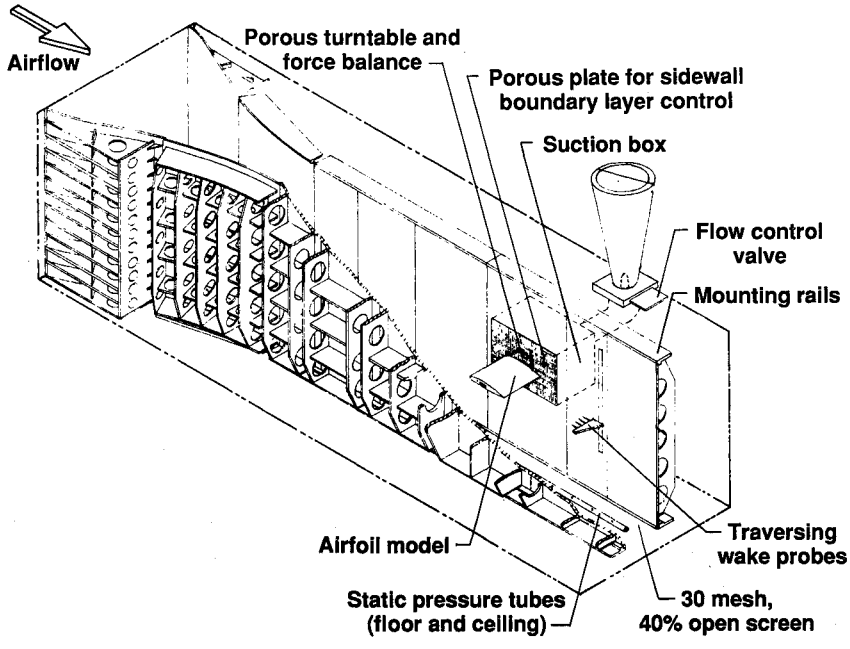

Fig. 2 Sketch of the NAE 15 × 60-in. Two-Dimensional High Reynolds Number Facility.

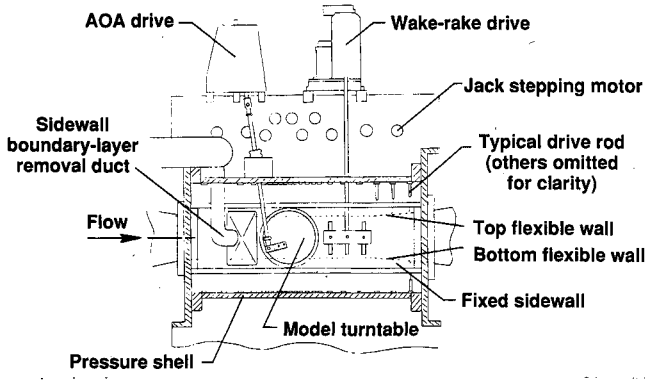

Fig. 3 Sketch of the NASA Langley 0.3-m Transonic Cryogenic Tunnel with the 13 × 13-in. adaptive-wall test section.

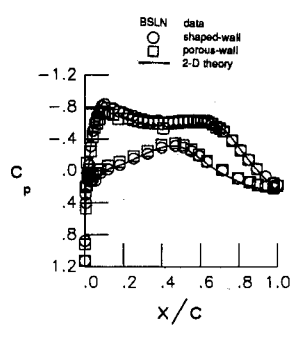

a) Pressure coefficient, $c_n \approx 0.4$

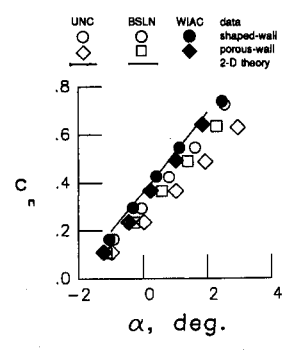

b) Normal force coefficient

Fig. 4 Comparison of results, $Re_c \approx 10 \times 10^6$ and $M \approx 0.700$.

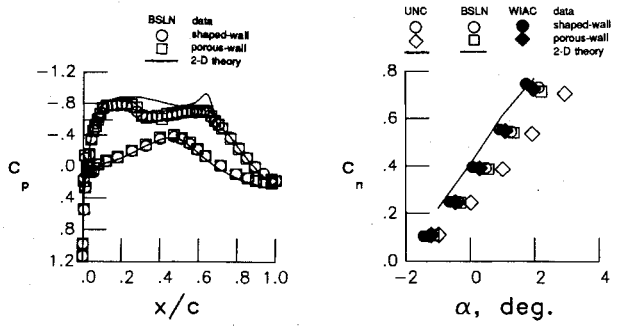

a) Pressure coefficient, $c_n \approx 0.4$ b) Normal force coefficient

Fig. 5 Comparison of results, $Re_c \approx 10 \times 10^6$ and $M \approx 0.750$.

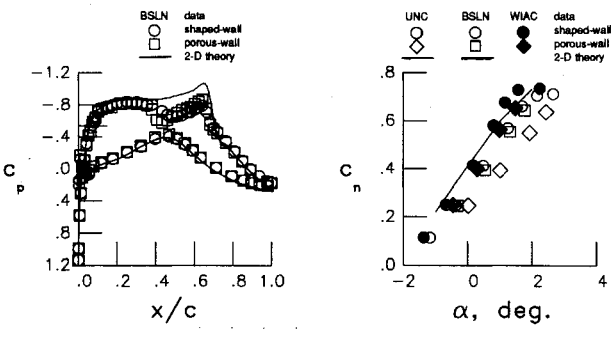

a) Pressure coefficient, $c_n \approx 0.4$ b) Normal force coefficient

Fig. 6 Comparison of results, $Re_c \approx 10 \times 10^6$ and $M \approx 0.765$.

both tests. The transition strip was located at the 5% chord location and was nominally 0.1 in. (0.25 cm) wide.

The model was tested over a wide range of Mach numbers and Reynolds numbers; this paper will focus on those tests at Mach numbers from 0.700 to 0.765 and at a chord Reynolds number of 10×10^6. The angle of attack was varied from about -2 deg through the stall angle. The angles of attack were chosen for the shaped-wall tests to obtain data at the same normal force coefficients as were obtained in the porous-wall tests.

Wall Interference Correction Techniques

Three types of wall interference correction techniques have been used. First, the potential flow technique was used to correct the porous-wall data for top and bottom wall interference. Second, the adaptive-wall technique was used to reduce the top and bottom wall interference in the shaped-wall tests by positioning the flexible walls. Third, the unified, four-wall, post-test transonic WIAC technique was used to correct the results from both tests. All of these techniques use measured data at or near the test section walls to determine the necessary corrections. The different correction techniques are summarized below.

Two-Wall Correction Technique

The porous-wall data[4] were corrected for top and bottom wall interference with the analytical technique of Mokry and Ohman.[5] This correction technique assumes that the flowfield near the test section boundaries can be represented by potential flow theory with linearized compressibility effects. The wall-induced streamwise disturbance velocity satisfies Laplace's equation within a rectangular control surface. The streamwise disturbance velocity on the control surface can be determined from the pressure distribution on the control surface, the model lift, and the model thickness; pressures along the upstream and downstream faces of the control surface are determined by interpolation. The resulting Dirichlet problem is solved using Fourier transform methods. Corrections to the model angle of attack and Mach number are computed at the quarter chord point of the model.

For the porous-wall data, the correction to angle of attack increases with normal force coefficient but is independent of Mach number. The correction to the Mach number increases with both the Mach number and the normal force coefficient.

Wall Adaptation Technique

The results[8] from the shaped-wall tests were "corrected" for top and bottom wall interference by the appropriate movement of the flexible walls, using the adaptation technique of Wolf and Goodyer.[9] This technique positions the top and bottom walls along free-air streamlines so that they do not interfere with the flow about the model. To accomplish this, the flowfield is split into two regions: a "real" flowfield inside a control surface and an "imaginary" flowfield extending from the control surface to infinity. The control surface is the effective wall position, that is, the physical wall position adjusted for the displacement thickness of the boundary layer. The wall position and the wall pressures are measured to determine the magnitude and direction of the real flowfield velocity. The flow at the control surface is assumed to be irrotational, inviscid, and subsonic; therefore, potential flow theory with linearized compressibility effects can be used to compute the imaginary flowfield. The difference between the measured and the computed flow magnitudes is used to compute several wall streamlining criteria. If all of the criteria are satisfied, the wall shape is considered to be a streamline. If they are not satisfied, the velocity differences along the boundary are used to predict a new wall position for another iteration.

Unified Wall Interference Correction Technique

The published results from each of the two tests, referred to herein as the baseline results, should be free from any significant top and bottom wall interference. Such interference in the porous-wall results[4] was corrected by a classical analytical technique.[5] The interference in the shaped-wall results[8] was reduced to what was deemed an acceptable level by the movement of the adaptive walls.[9] However, both sets of published results contain interference from the test section sidewalls, and the shaped-wall results could contain a small level of residual interference from the top and bottom walls. Clearly, all of the results should be as free as possible from any interference to approach free-air results.

A unified, four-wall, post-test, transonic WIAC procedure,[11-15] which can treat both shaped solid and porous planar top and bottom walls, has been applied to both data sets. The WIAC procedure involves a global iteration, each iteration or "pass" of which involves three solutions of the two-dimensional TSDE. In the first solution, the tunnel geometry is modeled and the Mach number is adjusted according to the Murthy sidewall boundary-layer approximation[14-16] while the TSDE is solved in an inverse fashion using measured wall and model pressures as boundary conditions. This step deduces an effective inviscid body shape that approximates the model and all of the viscous effects (even including separation and shock interaction with the boundary layers) on the model and all of the four tunnel walls. The second TSDE solution models free-air flow around this effective inviscid body while the Mach number and the angle of attack vary incrementally. This step determines the freestream Mach number and angle of attack for which the calculated free-air pressure coefficient distribution best matches the pressure coefficient distribution measured on the model during the test (including Mach number renormalization effects). The third TSDE solution uses the freestream conditions determined from the second solution and a source/vortex representation of the effective inviscid body from the first solution to determine the "classical-like" interference field.

The Neumann boundary conditions used in the two-dimensional TSDE solver require the upwash velocity component (in the x-z plane of Fig. 1) to be specified at the inflow

face of the test section to obtain a unique correction. In practice, the inflow upwash velocity component is rarely measured during airfoil tests, and no such flow measurement was made for the data considered in this paper. Thus, the upwash velocity component must be deduced iteratively, as previously demonstrated.[12-15] Up to three global iterations or "passes" of this procedure may be required to deduce the flow angularity at the inflow face of the test section and establish a unique boundary condition for the TSDE at the inflow face. These passes simultaneously act to properly align the computed effective inviscid body with the tested model.

Navier-Stokes Free-Air Calculations

The two-dimensional, free-air Navier-Stokes calculations presented in this paper were obtained from a code developed by Swanson and Turkel,[17] based on the explicit, finite-volume, multistage Runge-Kutta scheme for solving the Euler equations developed by Jameson et al.[18] The algorithm is formally second-order accurate except near shock waves where the controlled addition of dissipation[19] permits shock capturing without oscillations. This scheme has the highly desirable property that the steady-state solution is independent of the time step. The efficiency and robustness of this scheme has been successfully demonstrated.[19] Numerical efficiency is achieved by employing multigrid, local time stepping and implicit residual smoothing techniques to accelerate the convergence to a steady state. Computational efficiency is achieved through considerable vectorization of the computer code.[19] The turbulence model is a modified Baldwin-Lomax model.[20] All of the solutions were performed on a 320 × 64 C-mesh (128 points on the airfoil), with transition fixed at 5% of the airfoil chord.

The Navier-Stokes solutions provide an alternative assessment of the model pressure coefficient, normal- and drag-force coefficients for specified flow conditions. This assessment is independent of any wind-tunnel measurements and represents the current state of the art for computation of two-dimensional free-air flows at given flow conditions. When the Navier-Stokes solutions are compared to the wind-tunnel data, any differences between the two types of data should be attributable to correctable two-dimensional wall interference, to three dimensionality of the wind-tunnel flowfield, or to turbulence modeling, since other relevant flow physics are accurately modeled by the Navier-Stokes solution.

Aside from an independent assessment of the flowfield, the Navier-Stokes solutions also provide a set of fixed reference curves in the figures, which may aid in the assessment of the corrections that are applied to the wind-tunnel data. An argument can be made that comparisons between data and theory should be made only at the corrected flow conditions, but this necessarily complicates the presentation and assessment of the corrections, since each data point would then have a specific and unique Navier-Stokes curve for comparison. Also, since the data corrections are usually large relative to the effects of Mach number changes in the Navier-Stokes solution, improved data correlation is generally apparent with calculations performed at the nominal tunnel flow conditions. If the wall interference is sufficiently great, comparisons between the corrected wind-tunnel data and two-dimensional calculations, even at the corrected conditions, will not resolve all of the differences between these data sets, so the extra expense and effort required to make such comparisons may not be justified.

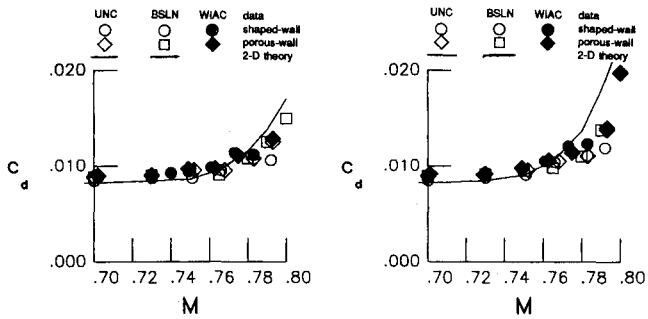

a) Drag force coefficient, $c_n \approx 0.2$ b) Drag force coefficient, $c_n \approx 0.4$

Fig. 7 Comparison of results, $Re_c \approx 10 \times 10^6$.

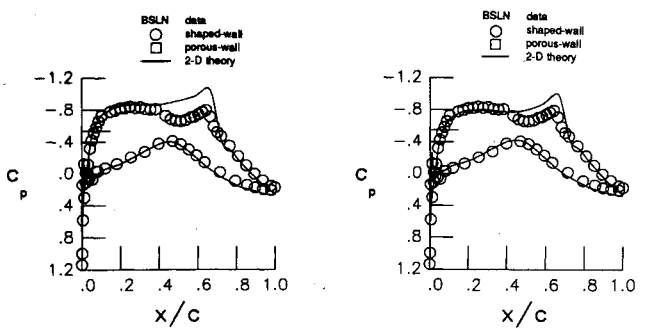

a) Pressure coefficient, uncorrected conditions b) Pressure coefficient, corrected conditions

Fig. 8 Comparison of results, $Re_c \approx 10 \times 10^6$ and $M \approx 0.765$.

Discussion of Results

Three types of figures with given Mach number, Reynolds number, and/or nominal normal force coefficient are presented. First are model chordwise pressure coefficient plots. Second are normal force coefficient vs angle of attack curves. Third are drag coefficient vs Mach number curves. The normal force coefficients have been deduced from the pressure coefficient, whereas the drag coefficients were obtained from wake-rake measurements taken behind the airfoil model.

The pressure coefficient plots reveal the structure of the flowfield on the model surface, including the placement of the shock, which strongly influences the correction procedure. The normal and drag force coefficient curves reveal more global characteristics of the flowfield, including the lift break and increased drag that accompany flow separation. Specifically, the normal force coefficient curves are intended to highlight the effects of angle of attack corrections, whereas the drag force coefficient curves are intended to highlight the effects of Mach corrections. These effects appear as horizontal translation of the data points in the respective curves; renormalization effects, which allow for proper comparison of the data at the corrected Mach number, appear as vertical translation of the data points in the curves. Another effect of the Mach correction is observed in the normal force coefficient curves, as the slope of the curve first increases, then decreases, with Mach number for the transonic flows considered here.

All results presented herein are at a Reynolds number of 10 × 10^6 based on the model chord of 9 in. (22.86 cm) and with transition fixed at the 5% chord location. The baseline shaped-wall results were used as inputs to the transonic WIAC technique. Uncorrected porous-wall results, that is, without the corrections of Mokry and Ohman, also were used as inputs to the transonic WIAC technique. Note in Figs. 4-8 that the symbol shape and symbol fill are used to distinguish the various data types. (On plots, BSLN refers to baseline data, UNC to uncorrected data.)

The results for a Mach number of 0.700 are presented in Figs. 4a and 4b. The three chordwise pressure distributions of Fig. 4a are in reasonably good agreement, although some differences exist, particularly on the upper surface of the airfoil. The baseline porous-wall data are shown at $M = 0.701$, $\alpha = 0.580$ deg, and $c_n = 0.366$; the baseline shaped-wall data are shown at $M = 0.704$, $\alpha = 0.800$ deg, and $c_n = 0.424$; the

Navier-Stokes results are shown for the nominal tunnel conditions of $M=0.700$, $\alpha=0.700$ deg, with $c_n=0.477$. The normal force coefficient vs angle of attack behavior is shown in Fig. 4b. As expected, the uncorrected porous-wall data and the baseline shaped-wall data differ considerably. The Mokry-Ohman correction that is used to obtain the baseline porous-wall results dramatically improves the correlation with the shaped-wall data, but the slopes and zero intercepts of the two baseline data sets still differ somewhat. Also, both baseline data sets differ noticeably from the Navier-Stokes free-air results. The WIAC corrections also shown in Fig. 4b improve the agreement between theory and experiment considerably. The slopes of all three data sets over the linear portion of the curve are in excellent agreement, although the curves are still displaced from one another. The WIAC correction moves the shaped-wall baseline data and the porous-wall uncorrected data to the left, which improves the correlation with the Navier-Stokes results.

The results at a Mach number of 0.750 are presented in Figs. 5a and 5b. The measured pressure coefficient distributions in Fig. 5a are in good agreement with each other but not with the Navier-Stokes results, especially on the upper surface. The baseline porous-wall data are shown at $M=0.751$, $\alpha=0.573$ deg, and $c_n=0.387$; the baseline shaped-wall data are shown at $M=0.750$, $\alpha=0.493$ deg, and $c_n=0.391$; the Navier-Stokes results are shown for the nominal tunnel conditions of $M=0.750$, $\alpha=0.500$ deg, and $c_n=0.509$. The disagreement between the computed and measured pressure coefficient distributions can be attributed to at least three causes. First, the Navier-Stokes calculations are performed at the baseline nominal tunnel Mach number and angle of attack, not the WIAC corrected Mach number and angle of attack. Second, the Navier-Stokes calculations were performed to simulate two-dimensional, free-air test conditions and the experimental measurements suggest that there were three-dimensional effects present in the experiment. Third, the turbulence model used in the Navier-Stokes calculations underpredicts the separation region of the flow, which allows the shock to move too far downstream. The agreement between the lower surface pressure coefficient is a good measure of how well the flow conditions have been matched for this sensitive airfoil.[21,22] The differences suggest that a residual correction to the Mach number and the angle of attack is needed. The agreement of the baseline section normal force coefficient data, shown in Fig. 5b, with each other is quite good. Again, the improvement in correlation of the porous-wall data with the Mokry-Ohman correction is quite noticeable, but the two baseline data sets differ considerably from the Navier-Stokes results. The WIAC corrections also shown in Fig. 5b again improve the correlation of the two data sets with the Navier-Stokes theory; over the linear portion of the curves, the agreement between the section normal force curve slopes is excellent; however, the curves are still displaced from each other. One shaped-wall data point at the highest c_n appears to have received too large of a correction; a similar phenomenon occurs as the Mach number is increased, and more discussion of this problem follows.

The results at a Mach number of 0.765 are presented in Figs. 6a and 6b. The chordwise pressure distributions are presented in Fig. 6a. As was found at a Mach number of 0.750, the baseline experimental pressure distributions are in good agreement with each other but not with the Navier-Stokes results. The baseline porous-wall data are shown at $M=0.766$, $\alpha=0.550$ deg, and $c_n=0.394$; the baseline shaped-wall data are shown at $M=0.766$, $\alpha=0.489$ deg, and $c_n=0.412$; the Navier-Stokes results are shown for the nominal tunnel conditions of $M=0.765$, $\alpha=0.500$ deg, and $c_n=0.504$. Although not shown, the differences in the pressure distributions increase as the Mach number or angle of attack increases. The agreement of the slopes of the section normal force curves, shown in Fig. 6b, is better between the two baseline results than between either one and the Navier-Stokes free-air results. The WIAC corrected results are also presented in Fig. 6b. As was the case at the lower Mach numbers, the slopes of the WIAC corrected results and the Navier-Stokes results are in excellent agreement at the low section normal force coefficients.

The point previously mentioned in Fig. 5b and the three shaped-wall data points in Fig. 6b with the highest c_n received large corrections and are moved to the left side of the Navier-Stokes curve. A similar problem was noted[23] for this CAST-10 data and also with NACA 0012 airfoil data[14] from the same facility at high lift coefficients and Mach numbers. The source of the correction problem, however, may well be physical rather than numerical. The correction problem coincides with the possible onset of three-dimensional flow in the test section at supercritical Mach numbers. A large spanwise gradient in the wake-rake drag coefficient for the shaped-wall data at these conditions suggests that three-dimensional flow is present in the test section. Similar analysis of the porous-wall wake-rake drag coefficient data at the same conditions showed much less of a spanwise gradient, probably due to the benefits of sidewall suction near the airfoil in the prone-wall tunnel. Moreover, for these high lift, transonic cases, the supersonic region begins near the leading edge where the sidewall boundary layer is thinning rapidly as the flow is expanding supersonically. The supersonic region terminates in a strong shock on the aft part of the airfoil, which may cause separation of the model and sidewall boundary layers. The characteristics for this supersonic region extend across the test section, nearly normal to the side walls; the characteristics are then reflected off a highly-shaped sidewall boundary layer to influence the flow at the midspan station, virtually independently of the tunnel width. The Murthy sidewall boundary-layer approximation used in the WIAC corrections assumed strictly subsonic flow at the wall and that the disturbances die off quickly in the spanwise direction as the tunnel width is increased. Moreover, the separation and three-dimensional flow described earlier can only be properly accounted for by a three-dimensional Navier-Stokes analysis.[23] The onset of three-dimensional flow cannot, however, be conclusively proven since no flow visualization is available in the 0.3-m TCT.

Additional normal force coefficient results[24] for Mach numbers of 0.78, 0.79, and 0.80 exhibit features similar to those of the Mach 0.765 case. The region of two-dimensional flow becomes smaller or nonexistent, and agreement with the Navier-Stokes results deterioriates as the Mach number and the normal force coefficient increase. These results, however, along with those of Figs. 4–6, were interpolated to determine the drag rise characteristics of the airfoil. The drag rise as a function of Mach number is presented in Figs. 7a and 7b for $c_n=0.2$ and 0.4, respectively. The level of drag measured in the two wind tunnels differed from each other and from the Navier-Stokes calculations. Also, the drag rise Mach numbers for the uncorrected and baseline experimental data are higher than for the Navier-Stokes data. Correlation is poor even between the baseline data sets above the drag rise Mach number. The WIAC corrections improve the correlation between the two measured data sets into the drag rise region and improve the correlation of the drag rise Mach number among all of the data sets. The WIAC corrections presented in Fig. 7, however, also include a buoyancy correction based on the streamwise pressure gradient through the tunnel.[25] The buoyancy correction increased with the Mach number and ranged from about 3 to 7 counts for the shaped-wall data and up to 2 counts for the porous-wall data. This significantly improved the correlation of the two measured data sets.

Point-by-point comparisons of the Navier-Stokes calculations at the corrected conditions, with the WIAC corrected data, improve the correlation between the data sets over the comparisons at the nominal conditions. One such comparison of the shaped-wall baseline and the Navier-Stokes computation chordwise pressure distribution (taken from Fig. 6a) is presented in Fig. 8a. As before, the baseline shaped-wall data are shown at $M=0.766$, $\alpha=0.489$ deg, and $c_n=0.412$; the

Navier-Stokes results are shown for the nominal tunnel conditions of $M=0.765$, $\alpha=0.500$ deg, and $c_n=0.504$. As noted previously, the Navier-Stokes solution is not in good agreement with the baseline results. Since the WIAC corrections suggested that the test conditions are different for the shaped-wall data, the Navier-Stokes solution[23] was computed at the corrected test conditions, as shown in Fig. 8b. The baseline shaped-wall data are again shown at $M=0.766$, $\alpha=0.489$ deg, and $c_n=0.412$; the Navier-Stokes results, however, are shown for the WIAC corrected tunnel conditions of $M=0.763$, $\alpha=0.174$ deg, and $c_n=0.442$. As expected, the results at the corrected test conditions are in better agreement than the results at the baseline test conditions. It is interesting to note that the design point of this airfoil is at $M=0.765$, and $c_n=0.6$, conditions well into the regime where three-dimensional flow effects may be observed.

The WIAC corrected angle of attack and Mach number were compared to the baseline angle of attack and Mach number. In general, the corrected angle of attack and Mach number were less than the corresponding baseline values. The difference between the corrected value and the baseline value increased with Mach number and angle of attack. The increment between the shaped-wall baseline and corrected value was from about 0 to about -0.6 deg for angle of attack and from about 0 to about -0.020 for the Mach number. Similarly, the increment between the porous-wall baseline and corrected value was from about 0 to -0.4 deg for angle of attack and from 0 to about -0.009 for the Mach number. These changes are slightly larger than those estimated[24] by a graphical technique involving the cross plotting of the mean and differential pressure coefficients at the airfoil quarter chord for various Mach numbers and angles of attack.

Concluding Remarks

A unified, four-wall interference assessment correction (WIAC) technique has been applied to the results from tests of a common airfoil model in two different types of test sections. The comparison of the baseline experimental results, the corrected experimental results, and the calculated Navier-Stokes results indicated the following:

1) The baseline results from the two tests were in reasonable agreement; however, some differences existed. Shaped-wall results had a larger normal force curve slope, a more negative angle of zero normal force, and a lower drag coefficient at a constant normal force coefficient. The uncorrected data sets differed significantly.

2) The WIAC procedure improved the agreement between the porous-wall and shaped-wall data with regard to the slopes of the section normal force curves and the drag rise Mach number.

3) The WIAC corrected data are in good agreement with the Navier-Stokes calculations on the linear portion of the section normal force curves at Mach numbers below the drag rise.

4) The WIAC corrected porous-wall data always correlated better with the Navier-Stokes results than did the comparable baseline data. The WIAC corrected porous-wall data also correlated better with the Navier-Stokes results at high lift and Mach number than did the WIAC corrected shaped-wall data, which indicates the benefits of the moderate sidewall suction used in the porous-wall facility to maintain two-dimensional flow with small, but correctable, four-wall interference.

5) The WIAC corrected shaped-wall data only correlated better with the Navier-Stokes results for lower lift levels and Mach numbers. At higher lift levels and Mach numbers, the corrections to the shaped-wall data were too large, due to inadequate modeling of the sidewall boundary layer for the supercritical three-dimensional flows. Presumably, only a three-dimensional Navier-Stokes analysis can properly account for the separation and three-dimensional flow that may exist in the adaptive-wall tunnel for high Mach numbers and normal force coefficient.

6) Mach number and angle of attack corrections predicted by the WIAC code were generally larger than those predicted[24] using the analysis of the quarter chord mean and differential pressures; better agreement between these two corrections existed for the porous-wall data than for the shaped-wall data.

7) The buoyancy correction, based on the streamwise pressure gradient through the tunnel, significantly improves the correlation between the measured drag sets.

Acknowledgments

The work described in this paper was conducted under a cooperative agreement between the National Aeronautical Establishment of Canada and NASA Langley Research Center. The purpose of the agreement was to investigate several different wall interference assessment/correction techniques. The authors wish to acknowledge Y. Y. Chan and his staff at the NAE High Speed Aerodynamics Laboratory for their efforts to design, build, and test the CAST-10 airfoil model and for making the results available under the cooperative agreement. The authors also wish to acknowledge R. C. Swanson of the NASA Langley Research Center for providing the Navier-Stokes analysis program and for assistance in interpreting the Navier-Stokes results.

References

[1]Seraudie, A., Blanchard, A., and Briel, J.F., "Rapport d'essais du Profil CAST 10 en Transition Declenchee Effectues dans la Soufflerie Transsonique Cryogenique T2 en Presence de Parois Auto-adaptables," ONERA R.T. OA 63/1685 AND, April 1985.

[2]Brown, D., "Information for Users of the National Research Council's 5 ft × 5 ft Blowdown Wind Tunnel at the National Aeronautical Establishment," National Research Council/National Aeronautical Establishment, Technical Rept., LTR-HA-6, 3rd ed., Ottawa, Ontario, Canada, Sept. 1977.

[3]Ohman, L. E., "The NAE High Reynolds Number 15 in. × 60 in. Two-Dimensional Test Facility. Part 1. General Information," National Research Council/National Aeronautical Establishment, Technical Rept. LTR-HA-4, Ottawa, Ontario, Canada, April 1970.

[4]Chan, Y. Y., "Wind Tunnel Investigation of the CAST-10-2/DOA-2 12% Supercritical Airfoil Model," National Aeronautical Establishment, Technical Rept. LTR-HA-5x5/0162, Ottawa, Ontario, Canada, May 1986.

[5]Mokry, M., and Ohman, L. H., "Application of the Fast Fourier Transform to Two-Dimensional Wind Tunnel Wall Interference," *Journal of Aircraft*, Vol. 17, No. 6, 1980, pp. 402–408.

[6]Ray, E. J., Ladson, C. L., Adcock, J. B., Lawing, P. L., and Hall, R. M., "Review of the Design and Operating Characteristics of the 0.3-Meter Transonic Cryogenic Tunnel," NASA TM-80123, Sept. 1979.

[7]Mineck, R. E., "Hardware and Operating Features of the Adaptive Wall Test Section Hardware for the Langley 0.3-Meter Transonic Cryogenic Tunnel," NASA TM 4114, June 1989.

[8]Mineck, R. E., "Wall Interference Tests of a CAST 10-2/DOA 2 Airfoil in an Adaptive-Wall Test Section," NASA TM 4015, Nov. 1987.

[9]Wolf, S. W. D., and Goodyer, M. J., "Predictive Wall Adjustment Strategy for Two-Dimensional Flexible Walled Adaptive Wind Tunnel—A Detailed Description of the First One Step Method," NASA CR-181635, Jan. 1988.

[10]Braslow, A. L., and Knox, E. C., "Simplified Method for Determination of Critical Height of Distributed Roughness Particles for Boundary Layer Transition at Mach Numbers from 0 to 5," NACA TN 4363, Sept. 1958.

[11]Kemp, W. B., Jr., "TWNTN4: A Program for Transonic Four-Wall Interference Assessment in Two-Dimensional Wind Tunnels," NASA CR-3777, Feb. 1984.

[12]Gumbert, C. R., "User Manual for the 0.3-m TCT Wall Interference Assessment/Correction Procedure, 8- by 24-inch Airfoil Test Section," NASA TM-87582, Sept. 1985.

[13]Green, L. L., and Newman, P. A., "Transonic Wall Interference Assessment and Corrections for Airfoil Data from the 0.3-m TCT Adaptive Wall Test Section," AIAA Paper 87-1431, June 1987.

[14]Green, L. L., "Wall Interference Assessment and Corrections for Transonic Adaptive Wall Data," M.S. Thesis, Mechanical Engineering Dept., George Washington Univ., Washington, DC, April 1988.

[15]Gumbert, C. R., "Wall Interference Assessment/Correction of Data from Tests of a CAST 10-2/DOA 2 Airfoil in the Langley 0.3-m

Transonic Cryogenic Tunnel," M.S. Thesis, Mechanical Engineering Dept., George Washington Univ., Washington, DC, May 1988.

[16]Murthy, A. V., "Effect of Aspect Ratio on Sidewall Boundary Layer Influence in Two-Dimensional Airfoil Testing," NASA CR 4008, Sept. 1986.

[17]Swanson, R. C., and Turkel, E., "A Multistage Time-Stepping Scheme for the Navier-Stokes Equations," NASA CR 172527, Feb. 1985.

[18]Jameson, A., Schmidt, W., and Turkel, E., "Numerical Solutions of the Euler Equations by Finite Volume Methods Using Runge-Kutta Time-Stepping Schemes," AIAA Paper 81-1259, June 1981.

[19]Swanson, R. C., and Turkel, E., "Artificial Dissipation and Central Difference Schemes for the Euler and Navier-Stokes Equations," AIAA Paper 87-1107, June 1987.

[20]Radespiel, R., and Swanson, R., "An Investigation of Cell Centered and Cell Vertex Multi-Grid Schemes for the Navier-Stokes Equations," AIAA Paper 89-0548, Jan. 1989.

[21]Swanson, R. C., and Schwanborn, D., "Some Navier-Stokes Calculations for the CAST-10 Airfoil," Second CAST 10 Workshop, Toulouse, France, Oct. 6-10, 1989.

[22]Thibert, J. J., and Rodde, A. M., "Theory-Experiment Comparisons," Second CAST 10 Workshop, Toulouse, France, Oct. 6-10, 1989.

[23]Swanson, R. C., Radespiel, R., and McCormick, V. E., "Comparison of Two- and Three-Dimensional Navier-Stokes Solutions With NASA Experimental Data for CAST 10 Airfoil," NASA CP 3052, Nov. 1989, pp. 233-258.

[24]Mineck, R. E., and Green, L. L., "Wall Interference Assessment/Correction (WIAC) for Transonic Airfoil Data from Porous and Shaped Wall Test Sections," AIAA Paper 90-1406, June 1990.

[25]Pope, A., and Harper, J. J., *Low-Speed Wind Tunnel Testing*, 1st ed., Wiley, New York, 1966, pp. 305-309.